Materials Today Chemistry 26 (2022) 101257

Contents lists available at ScienceDirect

Materials Today Chemistry

journal homepage: www.journals.elsevier.com/materials-today-chemistry/

Polyurethane foam scaffold for silica aerogels: effect of cell size on the mechanical properties and thermal insulation

B. Merillas [a, *], A. Lamy-Mendes [b], F. Villafañe [c], L. Durães [b], M.Á. Rodríguez-Pérez [a, d]

[a] Cellular Materials Laboratory (CellMat), Condensed Matter Physics Department, Faculty of Science, University of Valladolid, Campus Miguel Delibes, Paseo de Belén 7, 47011 Valladolid, Spain
[b] University of Coimbra, CIEPQPF, Department of Chemical Engineering, 3030-790 Coimbra, Portugal
[c] GIR MIOMeT-IU Cinquima-Química Inorgánica. Faculty of Science, University of Valladolid, Campus Miguel Delibes, Paseo de Belén 7, 47011 Valladolid, Spain
[d] BioEcoUVA Research Institute on Bioeconomy, University of Valladolid, Spain

ARTICLE INFO

Article history:
Received 12 July 2022
Received in revised form
14 October 2022
Accepted 19 October 2022
Available online 17 November 2022

Keywords:
Polyurethane foams
Nano-structures
Mechanical properties
Silica composites
Aerogel

ABSTRACT

Silica-based aerogels have been successfully reinforced by means of reticulated polymeric polyurethane (PU) foams with different cell sizes. The resultant silica aerogel-PU foam composites (Sil-PU composites) were fully characterized (density, shrinkage, aerogel percentage, and porous structure), and the mechanical properties and thermal conductivities were analyzed. Moreover, the effect of the application of a surface modification was assessed. A clear influence of the foam pore size on the final properties was found, and the mechanical properties of the aerogels have been notably improved reaching higher elastic modulus (from 130 to 307 kPa), excellent recovery ratios (above 95%), and significant deformations (more than 70%) without breaking. Therefore, the synthesized composites showed a great elasticity (high recovery ratios), tenacity, resilience, and stiffness in comparison with the non-reinforced aerogels. The obtained samples also showed excellent insulating capacities, reaching values between 14.0 and 12.3 mW/(m·K) for the surface-modified composites that were dried under supercritical conditions. Thus, using reticulated PU foams as a skeleton for aerogels is a promising strategy for a broad spectrum of applications in which silica aerogels are suitable candidates.

1. Introduction

Silica aerogels are open-porous materials generally synthesized through a sol-gel process. Their unusual properties point to them as suitable candidates for a wide range of scientific and industrial applications. Among their interesting properties are their high porosity (above 90%) and surface areas (~1000 m^2/g), really low densities (reaching values as low as 0.03 g/cm^3) and thermal conductivities (~15 mW/(m·K)), and high optical transmission (~ 80–90% in the visible region) [1–3]. Some of the applications in which silica aerogels can be employed are based on thermal superinsulation [4,5], catalysis [6], Cherenkov detectors [7], heavy metals, and oil adsorption [8,9] and in the aerospace sector as particle capturers, thermal insulators, cryogenic fluid containment, and fire retardants, among others [10,11].

Nevertheless, the main drawback of silica aerogels lies on their fragility, brittleness, and sensitivity at relatively low stresses [12]. For this reason, many works have focused their efforts on improving the mechanical properties of silica aerogels by different reinforcing techniques [13] such as polymer cross-linking [14,15], fiber incorporation [16–19], or the addition of carbon nanotubes [20–22], among others. One of the main drawbacks of these reinforcing strategies is the difficulty to disperse fillers homogeneously along the aerogel structure. For this reason, another interesting strategy is based on filling with aerogel a porous material that acts

Abbreviations: Sil-PU composites, (silica aerogel-polyurethane foam composites); PU, (polyurethane); TEOS, (tetraethoxysilane); CF, (carbon foam); HMDZ, (hexamethyldisilazane); BET model, (Brunauer–Emmet–Teller model); BJH, (Barrett–Joyner–Halenda); SCD, (supercritical drying); BSE, (backscattered electron detector); ELC, (energy loss coefficient); SEM, (scanning electron microscopy); Sil-SCD-M, (silica aerogel dried by supercritical conditions and modified with HMDZ); Sil-SCD, (silica aerogel dried by supercritical conditions and unmodified); C-SCD-M, (silica aerogel-polyurethane foam composite dried by supercritical conditions and modified with HMDZ); C-SCD, (silica aerogel-polyurethane foam composite dried by supercritical conditions and unmodified); S, M, and L, (small, medium, and large).

* Corresponding author.
E-mail address: b.merillas@fmc.uva.es (B. Merillas).

https://doi.org/10.1016/j.mtchem.2022.101257

as mechanical support. Schwan et al. [23] embedded aramid honeycombs into silica aerogels with the aim of improving their mechanical strength while keeping their low density and thermal conductivity. The selection of the used honeycomb material allows tailoring the final characteristics of the composites for their potential employment in new applications in which the aerogel fragility is the limiting factor. More recently, Liu et al. [24] prepared silica aerogel composites reinforced with an ultralight carbon foam (CF). The mechanical properties of the aerogels were significantly improved, and the thermal conductivity decreased in comparison with the initial foams (from 35 mW/(m·K) to 24 mW/(m·K)) since their cells were filled with a nanoporous material. Ye et al. [25] synthesized similar composites with a SiC coating through chemical vapor deposition over the CF, which promotes the aerogel introduction into the foam pores. Thus, a higher compressive response was reached as well as a better adiabatic insulation reducing the thermal conductivity of the initial foam up to 83% at 700 °C.

In this paper, we present a new composite material combining different formulations of silica aerogels based on tetraethoxysilane (TEOS) and several reticulated polyurethane (PU) foams. The use of PU foams provides several advantages over other materials. These foams are known for their cost-effectiveness, light weight, excellent mechanical properties, and thermal insulating capacity, being employed in a wide range of applications. Additionally, the polymeric skeleton acts as a homogeneous support for the silica aerogel matrix avoiding tedious dispersion procedures that usually lead to heterogeneous reinforcements. Finally, there is a wide variety of flexible foams with different densities and cell sizes; therefore, the PU foam can be selected according to the final requirements. The effect of the cell size on the final properties was assessed. The objective of this work is to provide an effective reinforcement through a proper selection of the polymeric skeleton that enhances the silica mechanical properties while maintaining their excellent insulating performance.

2. Materials and methods

2.1. Materials

Reticulated PU foams were provided by Recticel Ibérica, S.L. (Spain). Reticulated foams are characterized by having an open structure based on a continuous network of struts that forms the polyhedral pores and hold the skeletal structure [26]. The main characteristics of the PU foams used in this work are gathered in Table 1.

The synthesized silica aerogels are based on TEOS ($Si(OC_2H_5)_4$, 98%) supplied by Acros Organics. The acid and basic catalysts are oxalic acid ($C_2H_2O_4$, 99%) and ammonium hydroxide (NH_4OH, 25% NH_3 in H_2O), respectively, purchased from Fluka Analytical. Hexamethyldisilazane (HMDZ, $(CH_3)_3SiNHSi(CH_3)_3$, >98%), used as a silylating agent, was obtained from Alfa Aesar. For preparing the catalyst solutions (0.01 M of oxalic acid and 1 M of ammonium hydroxide), high-purity water was employed. Ethanol (EtOH, absolute, C_2H_5OH) was supplied by Fluka Analytical.

Table 1
Reticulated PU foam characteristics.

Foam	Density (Kg/m^3)	Cell size (μm)	Thermal conductivity (mW/(m·K))
S	29.39	435	38.25
M	29.17	1357	43.09
L	28.45	4291	47.40

2.2. Preparation of silica monoliths and Sil-PU composites

The TEOS-based monolithic aerogels were prepared in a two-step acid-base catalyzed sol-gel process. The silica precursor was dissolved in ethanol, and the solution was stirred at 300 rpm for 30 min after the addition of oxalic acid (0.01 M). Once the hydrolysis step is performed, the obtained solution is placed in an oven at 27 °C for 24 h. After this time, condensation was promoted by the addition of the basic catalyst (1 M), and the mixture was stirred at 300 rpm for 45 s. For the silica composites synthesis, the sol was poured into a glass beaker containing the reticulated PU foam until getting completely covered. After reaching the gelation time, the obtained silica monoliths and composites were placed into an oven at 27 °C for seven days, as described by previous procedures [18]. Finally, samples were demolded and washed twice with ethanol (2 × 12 h at 50 °C). For the samples in which the surface modification is performed, gels were covered with a mixture of 30% vol. of HMDZ in ethanol as solvent at 50 °C for 24 h. Then, gels were dried by supercritical drying (SCD) with CO_2 at 100 bar and 50 °C.

Composites with different dimensions were manufactured depending on the characterization technique that will be carried out: cylindrical composites with 12–16 mm of diameter and a height of around 10 mm for the mechanical experiments and 30–45 mm of cylindrical diameter and a height of 20–22 mm for the thermal insulation measurements.

2.3. Characterization techniques

2.3.1. Density, shrinkage, and aerogel mass

Density ρ was measured by dividing the mass of the samples (an AT261 MettlerToledo balance) by the geometric volume (with a caliper of 0.01 mm resolution) as described in ASTM (American Society for Testing and Materials) D1622/D1622M − 14 for apparent density of cellular plastics [27].

The aerogel's porosity (Π) was calculated by the Equation (1):

$$\Pi = (1 - \rho_r)*100 \quad (1)$$

where ρ_r is the relative density calculated by dividing the bulk density by the corresponding solid density (2.2 g/cm^3 [28]).

The linear (S_l) and volumetric (S_v) shrinkages were calculated to estimate the dimensional differences through the diameters or volumes, respectively, between the initial PU foam and the obtained final composites—Equations (2) and (3), respectively:

$$S_l(\%) = \left(1 - \frac{d}{d_0}\right) \cdot 100 \quad (2)$$

$$S_v(\%) = \left(1 - \frac{V}{V_0}\right) \cdot 100 \quad (3)$$

The aerogel mass percentage contained in the Sil-PU composites was assessed by equation (4):

$$\text{aerogel mass } (\%) = \frac{\left(m_{composite} - m_{foam}\right)}{m_{composite}}*100 \quad (4)$$

where $m_{composite}$ and m_{foam} are the mass of the composite and initial foam, respectively.

2.3.2. Nitrogen adsorption–desorption

The specific surface areas (S_{BET}) of the synthesized silica aerogels were determined by the nitrogen sorption technique through the use of the Brunauer–Emmet–Teller model. Measurements were carried out with a Micromeritics ASAP 2020 instrument at the

University of Malaga (Spain). Prior to the experiment, samples were degassed at 50 °C in a vacuum for 24 h to remove impurities. The pore size was calculated by the Barrett–Joyner–Halenda [29] method through the adsorption branch of the isotherms [29].

2.3.3. Scanning electron microscopy

Silica aerogels were cut and metalized through an iridium sputter coater (EMITECH K575X Sputter Coater) in order to avoid altering the microstructures [30]. For obtaining the micrographs, an Environmental scanning electron microscopy (ESEM) (QUANTA 200 FEG, Hillsboro, OR, USA) was employed.

In the case of the silica/PU composites, they were covered through a golden sputter coater, and the micrographs were obtained using a SEM (FlexSEM 1000, Hitachi), and for some of the micrographs, a backscattered electron detector was needed to improve the contrast resolution between both matrixes. The reticulated PU foams were visualized following the same procedure as for the composites, and their pore sizes were measured by software based on Image J/FIJI [31].

2.3.4. Mechanical properties

Uniaxial compression–decompression tests were performed with an Inspect mini-series (Hegewald & Peschke) at a strain rate of 1 mm/min. First, five cycles at a strain of 10% were performed by using a load cell of 50 N. An initial preload of 0.1 N was applied for all the experiments. Then, an additional compression–decompression cycle was carried out under the same conditions but reaching a strain of 25% to evaluate the elastic modulus. The recovery ratio (%) was measured by the initial height of the sample and the one reached after being compressed at 25%, for all the samples under study (Equation (5)).

$$25\%\ Recovery\ ratio = \frac{h_F}{h_0} \cdot 100 \tag{5}$$

being h_f and h_0 the final and initial heights, respectively.

Moreover, the energy loss coefficient (ELC) [32] was also calculated by means of the Equation (6):

$$\mathrm{ELC}\ (\%) = \frac{A_0 - A_F}{A_0} \cdot 100 \tag{6}$$

where A_0 and A_F are the area under the loading and unloading curve, respectively. The dimensions of the cylindrical composites were 12–16 mm of diameter and a height of ~10 mm.

After the compression–decompression tests, additional compression tests up to high strains were carried out with a heavier load cell (3 kN) until reaching a maximum load of 2.8 kN.

2.3.5. Thermal conductivity

The steady-state method has been used for measuring the thermal conductivity of the manufactured composites by a thermal heat flow meter FOX 314 (TA Instruments/LaserComp, Inc.) according to the normative ASTM C518 [33] and ISO 8301 [34]. To overcome the dimensional requirements that the thermal conductivimeter presents (a heat flux transducer of 100 × 100 mm^2), an external heat flux sensor gSKIN® XM 27 9C (greenTEG AG) (4.4 × 4.4 mm^2) in combination with a data logger gSKIN® DLOG-4219 (greenTEG AG) were coupled [35]. Two thermocouples were placed on both surfaces of the sample for monitoring the temperature during the heat transfer. The average temperature during the measurements was 10 °C, meaning that the hot plate was set at 20 °C, and the cold one at 0 °C. Both, silica aerogels and Sil-PU composites were measured by this method. The dimensions of the composites employed for these measurements were 30–45 mm in cylindrical diameter and a height of 20–22 mm. The silica aerogels were measured in powder form (using a mold) owing to the fragility and complexity of measuring them in the monolithic form without damage.

Since the PU foams presented a size larger than the transducer of the thermal heat flow meter FOX 314 (TA Instruments/LaserComp, Inc.), these samples were measured without any setup modification.

3. Results and discussion

In the following sections, the characterization of the initial PU foams and silica aerogels is presented. Then, the manufactured Sil-PU composites are studied in detail in terms of their density, linear and volumetric shrinkage, aerogel mass, and porous structure. Finally, the mechanical properties and thermal conductivities have been studied.

3.1. Polyurethane foams and silica aerogels characterization

In this study, reticulated PU foams have been used as support of different formulations of silica aerogels. Three PU formulations having different pore sizes have been employed (Fig. 1 a). Their porous structures have been visualized by scanning electron micrographs, as shown in Fig. 1 b, and their pore sizes have been measured obtaining 435 ± 62, 1357 ± 311, and 4291 ± 898 μm as average pore size values for the foams labeled as S (small), M (medium), and L (large), respectively.

The bulk density was similar for all the formulations being around 29 kg/m^3. Nevertheless, as said before, the difference between the average pore size is significant, covering a wide range of micrometer–millimeter scales to analyze the effect on the composite formation. Finally, their thermal conductivities have been measured showing values in agreement with their cell size. Since the density does not significantly change between samples, when the pore size is larger, the thermal conductivity increases owing to the higher radiation contribution since a lower amount of infrared radiation will be scattered. Additionally, convection mechanisms can take place owing to the large cell size of these foams. Thus, the obtained thermal conductivities are compressed between 38 and 47 mW/(m·K). These PU foams have been used as aerogel reinforcements by the formation of a gel (Fig. 1 c) that will be subsequently dried.

The silica-based aerogel monoliths were synthesized, and their bulk density and textural properties were analyzed. Additionally, the thermal insulating capacity of the pristine aerogels was also measured in powder form. These results can be found in Table 2.

There is a clear influence of the surface modification on the final density of the silica aerogels. The lowest density corresponds to the aerogel in which the surface modification with HMDZ has been applied (Sil-SCD-M) reaching a value of 79.2 kg/m^3. However, when the surface modification is not performed, density increases to 96.5 kg/m^3.

Regarding the textural properties, the surface areas obtained by nitrogen sorption are huge, with values from 700 to 781 m^2/g. The Barrett–Joyner–Halenda method was applied for measuring the pore size reaching pore sizes of 22 and 25 nm (modified and unmodified one, respectively). As depicted in Fig. 1 d, the silica aerogels were obtained as monoliths when the SCD is applied, whereas when the aerogels were dried under ambient pressure conditions, they broke immediately (not included in this work).

Finally, the thermal conductivity was measured. As expected, the non-modified sample presents a higher value of 20.95 mW/(m·K) since the solid contribution is slightly increased by the density rise. However, the modified aerogel showed a good

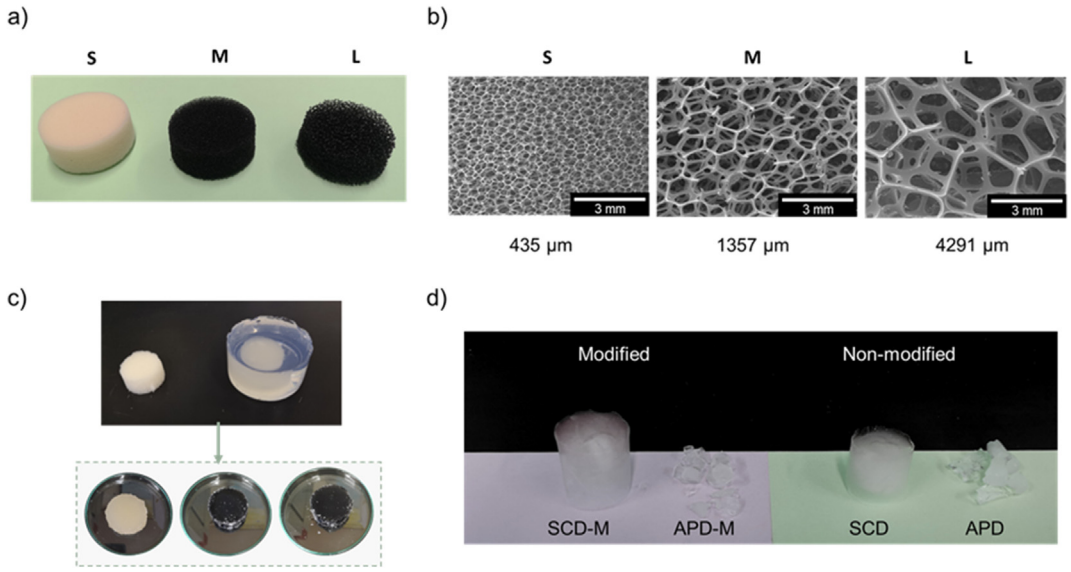

Fig. 1. (a) Reticulated polyurethane foams, (b) cellular structure micrographs of the polyurethane foams, (c) Sil-PU gels before the drying step, and (**d**) silica aerogels dried by supercritical drying with (modified) or without (non-modified) surface modification during the synthesis step.

Table 2
Silica aerogel characterization.

Properties	Sil-SCD-M	Sil-SCD
Bulk density (kg/m^3)	79.2 ± 2.7	96.5 ± 7.8
BET surface area (m^2/g)	700.0	781.3
BJH pore width (nm)	22	25
λ (mW/(m·K))	17.3 ± 1.4	21.0 ± 2.4

insulating value of 17.29 mW/(m·K). The aerogel modification has a strong impact on the final properties since the HMDZ acts as a silylating agent that increases the aerogel hydrophobicity and avoids shrinkage [18].

3.2. Composite characterization

The obtained composites were characterized in detail to assess the influence of the silica formulation as well as the effect of the foam pore size.

Fig. 2 displays the different composites synthesized for this work by using two different silica formulations (modified and non-modified) and three PU foams as support having different pore sizes (S, M, and L). Furthermore, these composites were synthesized at two sizes. Fig. 2 a shows the composites for the mechanical tests having dimensions of 12−16 mm of diameter and a height of around 10 mm, whereas Fig. 2 b shows the composites employed for the rest of properties (density, shrinkage, and thermal conductivity), which have larger dimensions.

In the following sections, the properties of the manufactured composites are analyzed.

3.2.1. Density, shrinkage, and aerogel mass

The bulk density of the produced composites, ranging between 98 and 134 kg/m^3, together with the shrinkages and mass of aerogel are summarized in Table 3. First, the difference between the modified and unmodified composites will be discussed hereafter.

- As previously seen for the silica aerogels, samples that were modified present a slightly lower density than the non-modified aerogels. Therefore, when comparing densities for the composites without modification (C-SCD) and the modified samples (C-SCD-M), the effect is clear: the surface modification promotes a reduction on the final bulk density of the composites. Consequently, linear and volumetric shrinkages are notably reduced reaching a decrease of 20% in some samples. The modified composites show a negative shrinkage meaning that the PU foams experiment an initial swelling of the silica sol; therefore, its size is larger (see Fig. 2 c). In this way, the shrinkage produced during the drying step is lower than the swelling mechanism, owing to the protection of the silanol groups that the hexamethyldisilazane (HMZD) produces. Nevertheless, when the aerogels are not modified, the hydroxyl groups on the aerogel surface may condense with each other resulting in a significant shrinkage.
- The amount of aerogel that is incorporated in the final composites slightly increases when the modification is performed. The HMDZ silylation promotes a better interaction with the PU matrix, and since there is a small amount of residual silanol groups, the structure resists structural rearrangements being more attached to the PU skeleton.

Finally, the influence of the cell size of the foams was assessed and analyzes as follows:

- As expected, the composite bulk density is lower when the size of the pores in which the aerogel is embedded is larger which means the S composites present the highest densities (117 and 134 kg/m^3 for the modified and non-modified composites, respectively), then, the M composites have intermediate densities (102 and 120 kg/m^3), and the largest pores, L composites, lead to composites with the lowest densities (98 and 112 kg/m^3). The main reason of this effect is related to the amount of silica aerogel that is able to fit inside the porous PU network. Therefore, when pores are smaller, the silica aerogel is more entrapped in the polymeric skeleton, whereas larger pores contribute to a more disconnected aerogel, which can be lost to some extent. The shrinkage trend is in agreement with the previous explanation: a higher shrinkage in the S composites is due to the more effective attachment to the PU struts, which are also shrunken (see Fig. 2), while the L composites have a

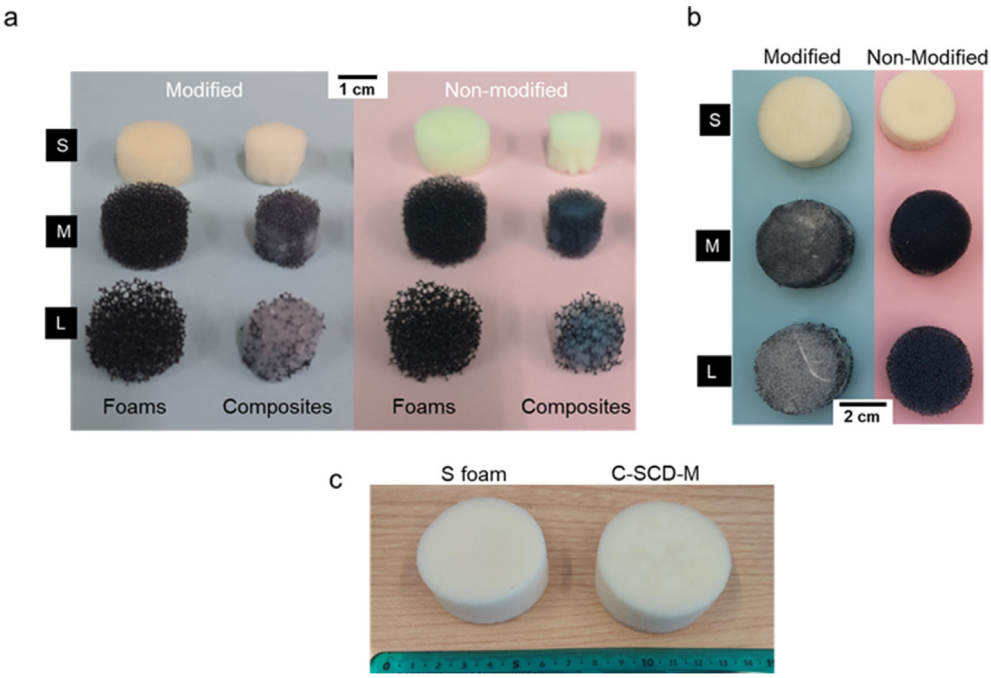

Fig. 2. Sil-PU composites for (a) mechanical properties, (b) thermal conductivity, and (c) picture showing the S foam and the corresponding modified composite.

larger amount of voids, avoiding the shrinkage when the aerogel does.

- According to the observation of the density and shrinkage trend, the amount of aerogel decreases as the pore size of the PU foam increases. For instance, for the modified composites, the percentage of aerogel goes from 82% for an S size, 77% for M size, and 74% for the largest pores L. In this work, the data show that, in general, the volumetric shrinkage are higher than the lineal one, indicating certain anisotropy for the materials under study. These differences are higher for the C-SCD-M samples.

3.2.2. Porous structure

The porous structure of the synthesized composites was analyzed by means of SEM.

Since the composite with the lowest density and shrinkage was found to be the sample in which the surface modification had been performed (C-SCD-M), the SEM micrographs of this composite have been obtained for all the pore sizes (the rest of sample images can be found in Fig. S1). The obtained pictures can be found in Fig. 3.

Table 3
Density, shrinkage, and the aerogel mass for the synthesized Sil-PU composites.

Sample	Properties	C-SCD-M	C-SCD
S	Density (kg/m^3)	117.7	134.1
	Linear shrinkage (%)	−8.4	7.0
	Volumetric shrinkage (%)	−30.8	12.5
	Aerogel mass (%)	82.1	76.0
M	Density (kg/m^3)	102.1	120.4
	Linear shrinkage (%)	−4.7	6.5
	Volumetric shrinkage (%)	−23.5	7.0
	Aerogel mass (%)	77.4	75.3
L	Density (kg/m^3)	98.5	112.6
	Linear shrinkage (%)	−2.1	7.2
	Volumetric shrinkage (%)	−15.5	9.0
	Aerogel mass (%)	74.8	72.8

A noticeable effect of the pore size can be observed for the foam with the smallest pore size (S), the silica aerogel forms a continuous solid network, and it is completely entrapped into the reticulated polymeric skeleton. For the medium pore size (M), some air voids are found as a result of small disconnections between the aerogel and the struts causing a slight loss of aerogel as it was assessed in the previous section; when the pore size is further increased, L, these voids are more remarkable giving account for the cracks that the aerogel experiments and a larger amount of aerogel is lost.

3.2.3. Mechanical properties

First, uniaxial compression experiments using a load cell of 3 kN were performed for the reference PU foams, the pure silica aerogels, and the Sil-PU composites. The obtained composites do not break; they only experiment a densification process (Fig. 4 a) in which the silica nanoparticles are forced to reduce the air voids between them. Regarding the different silica formulations, the composite with the HMDZ modification shows the greatest deformations reaching values near 100%. Nevertheless, the unmodified composites are able to support a lower strain of around 70%, and the stress needed for reaching these deformations is higher. Fig. 4b shows the strain−stress curves for the reticulated PU foams. Three different regions can be differentiated along these curves: an initial region in which the elastic deformation takes place until around 10%, then, a plateau region appears covering a wide range of strains (from 10 to 60%), and finally, a strong densification occurs from 70% on. The cell size seems not having a significant effect on the deformation capacity of these composites.

Despite the synthesized composites do not show any break, having excellent deformation capacities, the silica aerogel (Sil-SCD-M) was broken at a strain of 12% (Fig. 4c). Thus, the PU reinforcement has significantly improved the silica aerogel mechanical properties allowing to obtain a more stable structure which does not break. When using other foams as support for producing silica aerogel composites, as those reported by Liu et al. [24] or Ye et al. [25], compressive forces led to cracks on the silica aerogel that are not present in this work.

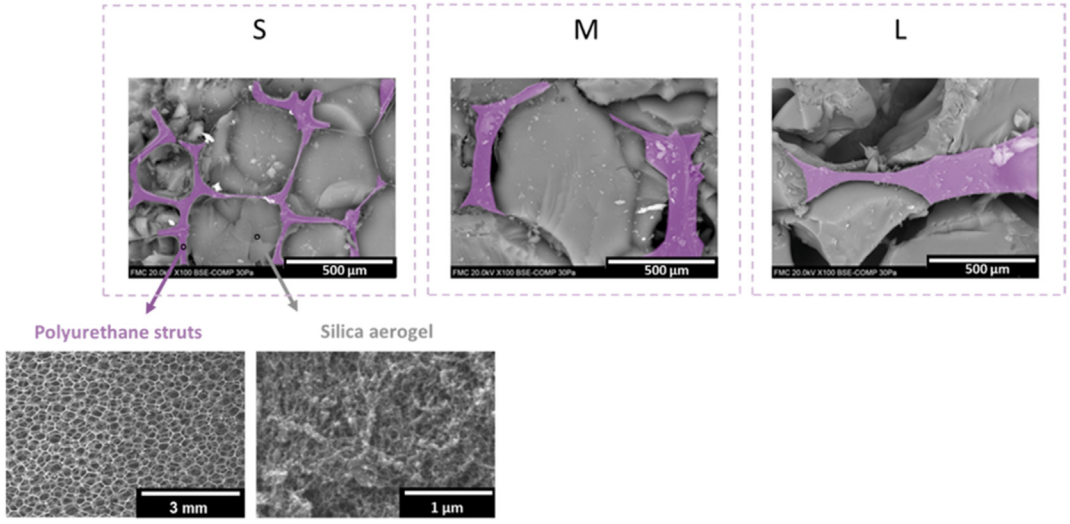

Fig. 3. Scanning electron micrographs for the modified composite (C-SCD-M) with the polyurethane foams S, M, and L. SCD, supercritical drying.

From these curves, the corresponding values of stress at different strains were obtained and normalized with the sample density to remove its effect (Table 4), (Fig. S1). In general, the non-modified composites showed higher stress for each strain (25, 50, and 75%) than the modified ones. Regarding the cell size of the PU foams a clear trend is noticed, the larger the pores, the higher the stress.

Afterward, a compression–decompression cycle was performed until reaching a 25% of strain (Fig. 5). From these curves, the recovery ratio and the elastic modulus were calculated in the elastic region (5–10%). Since the manufactured composites showed a wide range of densities, prior to the assessment of the obtained results, the elastic modulus was normalized by means of the bulk density to remove its influence. The obtained values are gathered in Table 4 (raw values without the normalization can be found in Table S2).

Regarding the recovery ratio, all the composites show recoveries higher than 95% giving account for their excellent elasticity and resilience.

Taking into account the normalized elastic modulus (see Supporting Information Fig. S1), except for the smallest pores, the M and L composites are the modified formulation which presents the highest elastic modulus. When comparing the elastic modulus of the modified composites with that of the silica monolith, there is a significant increase for the composites. In this way, the stability and stiffness of the reinforced aerogel are notably improved when the surface modification is applied (enhancements of more than a 75% were reached for the modified composites, from 130 kPa to ca. 230 kPa). This experiment could not be carried out for any of the aerogel formulations due to the aerogels breakage, as explained before.

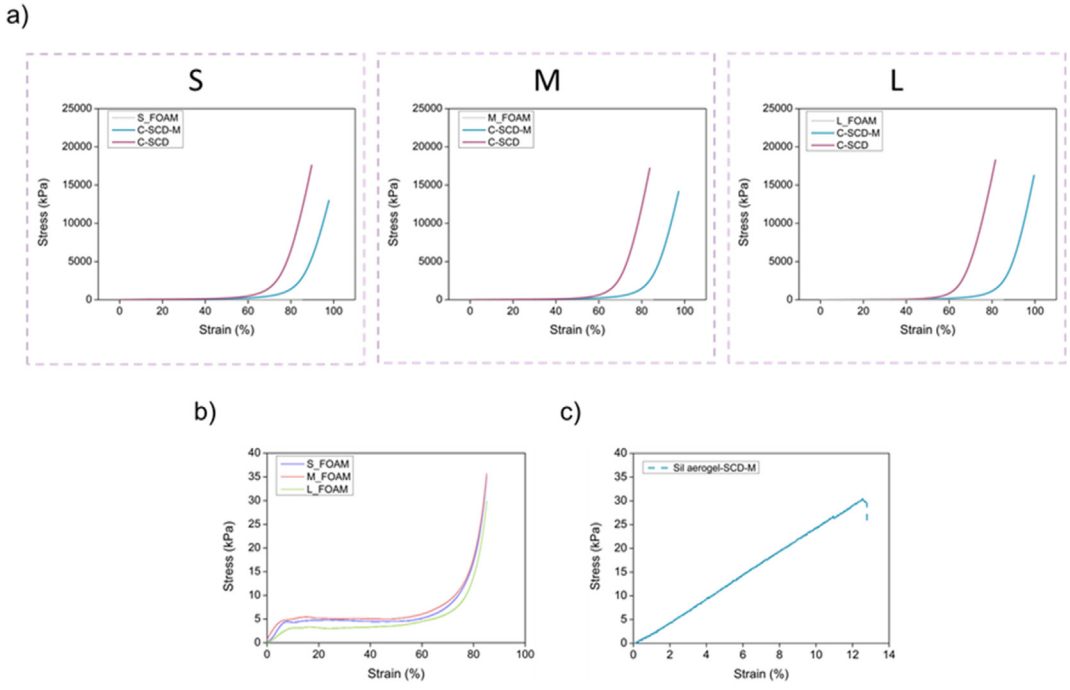

Fig. 4. Stress–strain curves for the (a) composites, (b) foams, and (c) silica aerogel, obtained by compression with a load cell of 3 kN.

Table 4
Mechanical parameters obtained from the compression–decompression curve at 25% of strain (elastic modulus and recovery ratio) and from the compression tests up to high strains (stress at different strains) normalized by the sample density.

Sample	Properties	PU Foam	C-SCD-M	C-SCD
S	(25%) Recovery ratio (%)	97.9	97.9	95.7
	Elastic modulus/ρ (kPa·m^3/kg)	0.744	2.260	3.272
	$\sigma_{25\%}$/ρ (kPa·m^3/kg)	0.163	0.494	0.765
	$\sigma_{50\%}$/ρ (kPa·m^3/kg)	0.153	1.497	2.468
	$\sigma_{75\%}$/ρ (kPa·m^3/kg)	0.367	8.841	34.212
M	(25%) Recovery ratio (%)	97.7	96.0	99.3
	Elastic modulus/ρ (kPa·m^3/kg)	0.685	2.847	1.336
	$\sigma_{25\%}$/ρ (kPa·m^3/kg)	0.175	0.624	0.521
	$\sigma_{50\%}$/ρ (kPa·m^3/kg)	0.175	1.656	2.452
	$\sigma_{75\%}$/ρ (kPa·m^3/kg)	0.394	9.841	72.513
L	(25%) Recovery ratio (%)	100	99.5	97.1
	Elastic modulus/ρ (kPa·m^3/kg)	0.329	2.824	1.235
	$\sigma_{25\%}$/ρ (kPa·m^3/kg)	0.105	0.614	0.331
	$\sigma_{50\%}$/ρ (kPa·m^3/kg)	0.127	1.438	2.589
	$\sigma_{75\%}$/ρ (kPa·m^3/kg)	0.295	8.072	120.605

Additionally, the ELC (%) was calculated through the area under the stress–strain curves of Fig. 5. These values can be found in Table 5.

The PU foams showed ELCs that vary from 59 to 54% as the pore size is larger. This trend is practically maintained for all the composites. In this way, the L composites showed the smallest hysteresis, and a lower amount of energy is dissipated during the compression–decompression experiment. Therefore, these composites are more elastic than the S and M ones, which suffer a slight plastic deformation in agreement with the previously analyzed recovery ratios. Comparing the samples in which the surface modification is applied with those without this step during their synthesis, the ELCs are significantly reduced reaching values as low as 42%. These samples dissipate the minimum energy and present a more elastic behavior during the load–unload cycle.

Finally, five additional compression–decompression cycles were carried out until reaching a strain of 10%. The graphs obtained during these experiments are displayed in Fig. 6. In the first row, the results for the three PU foams are presented (grey color). It is clearly observed that all of them show an elastic behavior, and the stress needed for reaching a deformation of 10% is higher when the pore size increases. The maximum value of stress for the S foam is ca.4 kPa, whereas for the M and L foams this value is around 6 kPa and 8 kPa, respectively. In the following rows, the composites behavior is presented. In general, the stress for deforming to 10% of strain is higher for the composites with lower cell size since the corresponding density is higher too.

When assessing the effect of the surface modification step, the results of this experiment are not conclusive. Nevertheless, it can be affirmed that all the manufactured composites have an elastic behavior when a deformation of 10% is applied.

3.2.4. Thermal conductivity

The steady-state method has been employed for measuring the insulating capacity that the composites present [36]. First, the initial PU foams and pristine silica aerogels were characterized in terms of their thermal conductivity as described in Section 3.1. Then, this property was measured for the Sil-PU composites obtaining the following results plotted in Fig. 7 a (the numerical values can be found in Supporting Information Table S2). There is a clear decrease in the initial foam conductivity when the silica phase is incorporated. The different factors affecting this property are analyzed hereafter:

- Effect of surface modification: when comparing the thermal conductivities of the modified samples with the non-modified ones, a huge difference can be observed. The modified samples (blue color) show lower thermal conductivities than the corresponding samples in which this modification has not taken place (pink color), which indicates the influence of this modification in the cohesion between both matrixes.
- Effect of foam pore size: all the formulations follow the same trend regarding the pore size of the initial PU foam. For the non-modified composites, the thermal conductivity decreases from 30.9 mW/(m·K) for the S size to 17.0 and 21.9 mW/(m·K) for the M and L sizes, respectively. When the modification is applied, thermal conductivity goes from 14.0 mW/(m·K) for S foam to 13.0 mW/(m·K) for M foam and reaches the lowest value of 12.3 mW/(m·K) for the L foam.

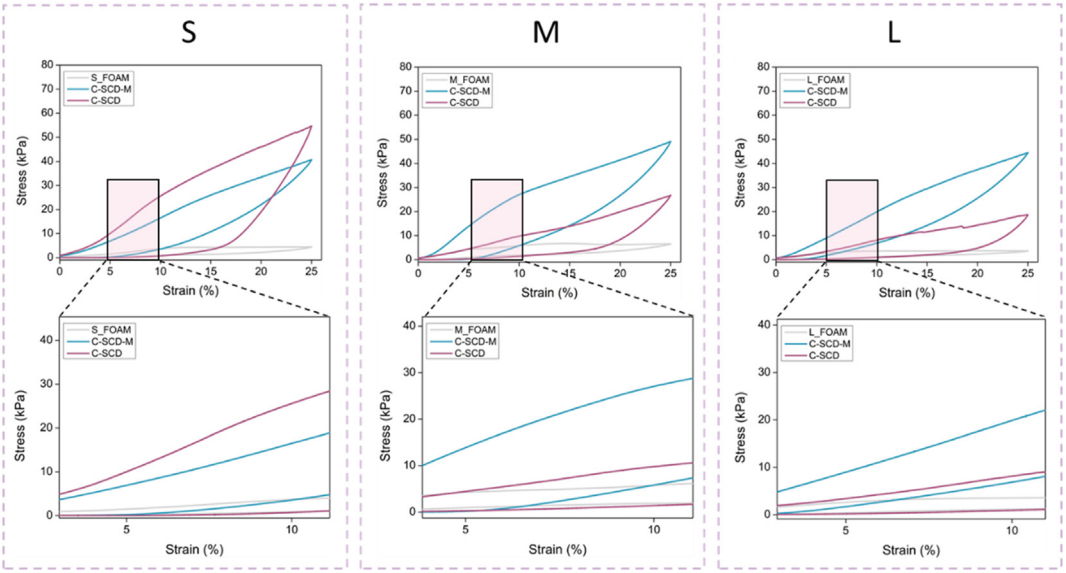

Fig. 5. Compression–decompression cycle for the polyurethane foams and Sil-PU composites at a strain of 25%. PU, polyurethane.

Table 5
Energy loss coefficients obtained from the compression–decompression curves at 25% of strain.

Sample	Properties	PU Foam	C-SCD-M	C-SCD
S	ELC (%)	59.8	46.9	68.5
M	ELC (%)	55.7	46.0	61.5
L	ELC (%)	54.3	42.7	68.3

These results agree with the previous characterization. Since the S composites showed the highest densities, the solid contribution to the total thermal conductivity will be increased. The thermal conductivities reached for the M and L composites are similar.

Moreover, when comparing the values for the composites with those of the PU foams, a clear decrease is found. Despite the rise in the final density when the silica phase is included in the structure, the gaseous contribution reduction is stronger. In this way, when the macropores are filled with the silica aerogel showing pores in the nanometric scale, the well-known Knudsen effect [37] takes place, and the gaseous conduction is significantly reduced.

If the initial values of the pure silica-based aerogels are compared with those of the reinforced composites, an interesting observation can be done. For the Sil-SCD-M aerogel, the obtained thermal conductivity value was 17.3 mW/(m·K). When this formulation is reinforced with the reticulated foams, the C-SCD-M composites reached the lowest thermal conductivities: 14.0, 13.1, and 12.3 mW/(m·K) at S, M, and L foam pore size, respectively. In the case of the non-modified Sil-SCD aerogel (21 mW/(m·K)), the corresponding composites achieved a similar thermal conductivity at M and L size, while that of the S composite is higher. It has to be taken into account that the initial silica formulation was measured in powder form, i.e. that the voids between the silica powder are increasing the initial thermal conductivity.

Liu et al. [24] and Ye et al. [25] used the same strategy by synthesizing CF/silica aerogel composites reaching thermal conductivities of 24 and 32 mW/mK, respectively. Therefore, the choice of PU foams as a scaffold for silica aerogels constitutes a better alternative than other porous supports to keep the low thermal conductivity of the silica aerogel.

In conclusion (see Fig. 7b and c), the application of a surface modification with HMDZ promotes the best interaction between silica and PU matrixes and contributes to the aerogel stability, which is necessary for achieving really low thermal conductivities while improving the mechanical properties. Moreover, a pore size around 1300 μm (M size) would provide the best samples in terms of properties (thermal and mechanical) and a stable and interconnected porous structure.

With the aim of comparing the obtained thermal conductivities with the theoretical ones, the rule of mixture was applied as previously done for similar silica-based composites [23] but in a parallel model:

$$\frac{1}{\lambda_{eff}} = \frac{\chi_{aerogel}}{\lambda_{aerogel}} \cdot + \frac{\chi_{PU}}{\lambda_{PU}} \quad (7)$$

where λ is the thermal conductivity of the silica aerogel or solid PU, and χ is the mass fraction of each component.

By assuming that the whole porosity of the PU foams (ca. 97%) is filled with the silica aerogels, the estimated thermal conductivity would be of 17.8 mW/(m·K) for the C-SCD-M composite and 21.5 mW/(m·K) for the unmodified one, which are the same values than the measured for the silica aerogels (17.3 and 20.9 mW/(m·K), respectively). This last statement explains that, in an ideal situation,

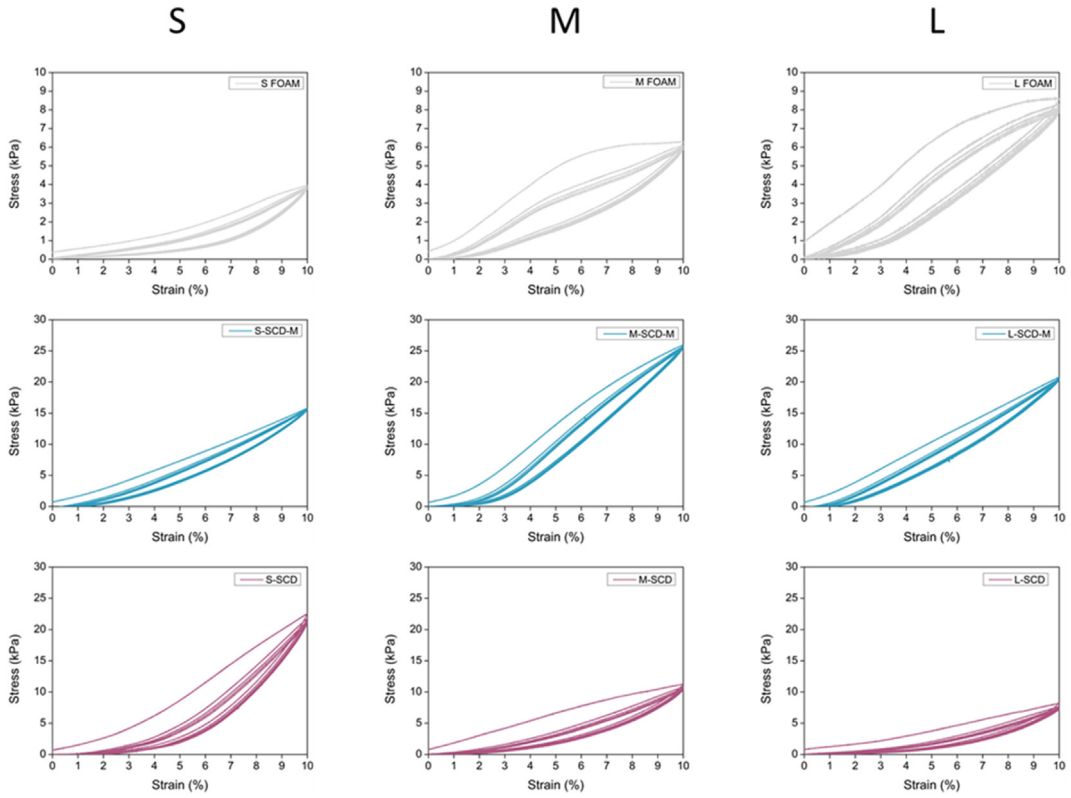

Fig. 6. Compression–decompression cycles up to 10% of strain for the initial PU foams and the manufactured composites.

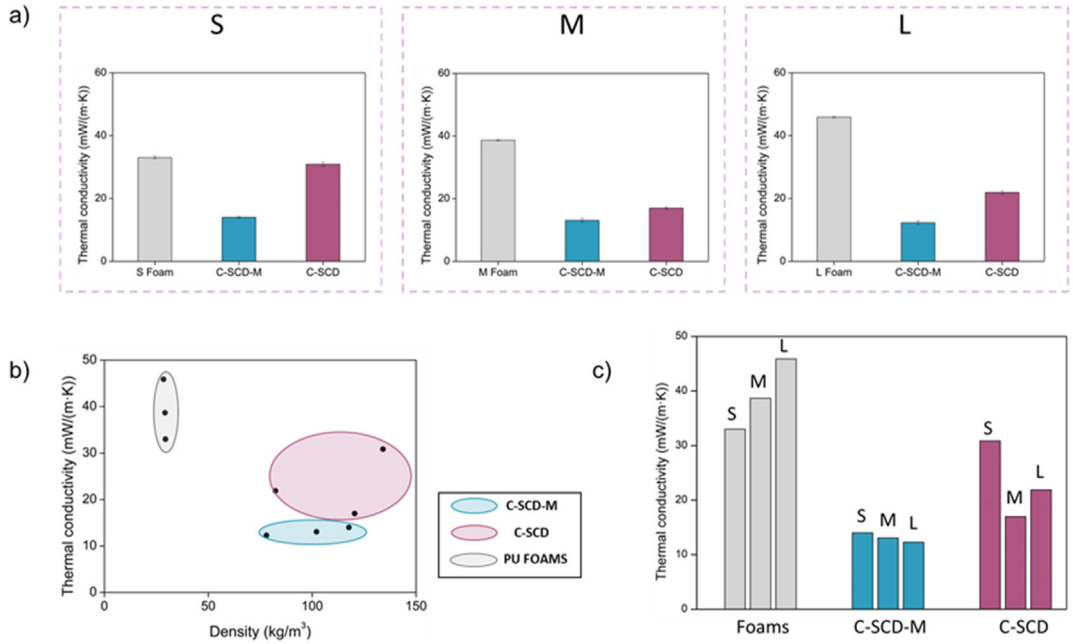

Fig. 7. (a) Thermal conductivities obtained for the polyurethane foams and silica-polyurethane composites, (b) Thermal conductivity—density relationship for all the samples under study, and (c) Thermal conductivity classified into the type of samples under study.

heat would be transferred through the aerogel phase since the volume fraction of the PU skeleton is really low (0.03%), and the network which it forms is completely covered by a continuous phase of silica aerogel. These values are slightly higher than those obtained for the corresponding composites since the silica aerogels were measured in powder form; thus, the conduction through the gaseous phase between the powder particles is increasing the final value.

4. Conclusions

Silica reinforced composites have been synthesized by using reticulated PU foams as a strategy to improve their stability and mechanical properties. Different factors were analyzed in order to find the optimum conditions, formulation and reinforcement. In this way, the silica aerogel formulation was modified through surface modification with HMDZ and foams having different pore sizes (S, M and L) were used.

Density changes with the different studied parameters. The surface modification promotes a more stabilized structure, and the density of these samples is slightly lower. Furthermore, the pore size of the PU foams has a strong influence, diminishing the final density of the composites when the pore size is increased. The percentage of silica aerogel included in the final composites is really high obtaining values from 72 to 82%.

The porous structure assessment reveals that the S foams contribute to the formation of an effective cage for the silica aerogel, which is forming a continuous solid network. When the foam pore size increases, the silica aerogel breaks more easily, and some voids between the PU skeleton and the silica aerogel appear.

Regarding the mechanical properties of the manufactured composites, different compression tests were carried out. The Sil-PU composites showed a significantly elastic behavior at deformations of 10 and 25%, reaching recovery ratios above 95%. The composites present a higher elastic modulus than the corresponding pure silica aerogel when the HMDZ modification was performed. This value increases from 130 to 307 kPa (C-SCD-M at S size) obtaining stiffer samples. Then, the ELC was calculated and the L composites were those which showed the minimum dissipated energy during the compression—decompression tests and thus the more elastic composites. Finally, samples were compressed until high values. While the pure aerogel was broken at a strain of 12%, the Sil-PU composites reached values near 100% without breaking, and only densification was observed. This fact gives account for the stiffer and more elastic properties that the aerogels show when reinforced with this polymeric matrix.

The thermal conductivities were also measured, and the different affecting parameters were assessed. The greatest insulating performance was reached for the modified composites at a pore size of M and L, reaching 13.0 and 12.3 mW/(m·K), respectively.

Not only do these values confirm the effectiveness of the silica reinforcement through a reticulated PU foam improving their stiffness, tenacity, and porous structure but they also keep really low thermal conductivities not achieved before. Thus, reticulated PU foams provide a reinforcement for silica aerogels that significantly improves their pristine properties and is superior to other alternatives previously reported.

Funding

Financial support from the FPU grant FPU17/03299 (Beatriz Merillas) from the Ministerio de Ciencia, Innovación y Universidades (RTI2018-098749-B-I00) is gratefully acknowledged. Financial assistance from the Junta de Castilla y León (VA202P20) and the “Ente Público Regional de la Energía de Castilla y León" (EREN) are gratefully acknowledged. This work was supported by the Regional Government of Castilla y León and the EU-FEDER program (CLU-2019-04).

This work was also developed under the workplan of the Short-Term Scientific Mission (STSM) grant No 47454, within the scope of the COST-Action “Advanced Engineering of aeroGels for Environment and Life Sciences” (AERoGELS, Ref. CA18125) funded by the European Commission.

Work developed at CIEPQPF (Chemical Process Engineering and Forest Products Research Centre) funded through projects UID/EQU/00102/2020 and by national funds via the Portuguese Foundation for Science and Technology (FCT).

Author contributions

Conceptualization, Beatriz Merillas, Alyne Lamy-Mendes, Fernando Villafañe, Luisa Durães and Miguel Rodríguez-Pérez; Data curation, Beatriz Merillas; Formal analysis, Beatriz Merillas; Funding acquisition, Fernando Villafañe, Luisa Durães and Miguel Rodríguez-Pérez; Investigation, Beatriz Merillas and Alyne Lamy-Mendes; Methodology, Beatriz Merillas, Alyne Lamy-Mendes, Luisa Durães and Miguel Rodríguez-Pérez; Project administration, Fernando Villafañe, Luisa Durães and Miguel Rodríguez-Pérez; Resources, Fernando Villafañe, Luisa Durães and Miguel Rodríguez-Pérez; Software, Beatriz Merillas; Supervision, Fernando Villafañe, Luisa Durães and Miguel Rodríguez-Pérez; Validation, Fernando Villafañe, Luisa Durães and Miguel Rodríguez-Pérez; Visualization, Fernando Villafañe, Luisa Durães and Miguel Rodríguez-Pérez; Writing – original draft, Beatriz Merillas; Writing – review & editing, Beatriz Merillas, Alyne Lamy-Mendes, Fernando Villafañe, Luisa Durães, and Miguel Rodríguez-Pérez.

Declaration of competing interest

The authors declare that they have no known competing financial interests or personal relationships that could have appeared to influence the work reported in this paper.

Data availability

Data will be made available on request.

Acknowledgments

The authors would like to thank María Dolores Marqués Gutiérrez, from the Porous Solids Laboratory of the University of Malaga, for the nitrogen adsorption measurements. The authors would like to thank to Alberto Santiago Aliste, from the Unidad de Microscopía of the Parque Científico of the University of Valladolid, for the HR-SEM measurements and Pablo Obregón Sandoval for the SEM (FlexSEM 1000, Hitachi) measurements.

Appendix A. Supplementary data

Scanning electron micrographs for the non-modified composites (C-SCD), the elastic modulus and normalized elastic modulus of al the samples, the stress at 25%, 50% and 75% of strain for the PU foams and composites, as well as the thermal conductivities at 10 °C are included in the Supporting Information.

Supplementary data to this article can be found online at https://doi.org/10.1016/j.mtchem.2022.101257.

References

[1] M.A. Aegerter, N. Leventis, M.M. Koebel, Aerogels Handbook, Springer, Berlin, Germany, 2011, https://doi.org/10.1007/978-1-4419-7589-8_4.
[2] A. Venkateswara Rao, S.D. Bhagat, H. Hirashima, G.M. Pajonk, Synthesis of flexible silica aerogels using methyltrimethoxysilane (MTMS) precursor, J. Colloid Interface Sci. 300 (2006) 279–285, https://doi.org/10.1016/j.jcis.2006.03.044.
[3] A. Venkateswara Rao, S.D. Bhagat, Synthesis and physical properties of TEOS-based silica aerogels prepared by two step (acid-base) sol-gel process, Solid State Sci. 6 (2004) 945–952, https://doi.org/10.1016/j.solidstatesciences.2004.04.010.
[4] K. Duer, S. Svendsen, Monolithic silica aerogel in superinsulating glazings, Sol. Energy 63 (1998) 259–267, https://doi.org/10.1016/S0038-092X(98)00063-2.
[5] J. Wang, D. Petit, S. Ren, Transparent thermal insulation silica aerogels, Nanoscale Adv. 2 (2020) 5504–5515, https://doi.org/10.1039/d0na00655f.
[6] J.E. Amonette, J. Matyáš, Functionalized silica aerogels for gas-phase purification, sensing, and catalysis: a review, Microporous Mesoporous Mater. 250 (2017) 100–119, https://doi.org/10.1016/j.micromeso.2017.04.055.
[7] M. Tabata, P. Allison, J.J. Beatty, S. Coutu, M. Gebhard, N. Green, D. Hanna, B. Kunkler, M. Lang, K. McBride, S.I. Mognet, D. Müller, J. Musser, S. Nutter, N. Park, M. Schubnell, G. Tarlé, A. Tomasch, G. Visser, S.P. Wakely, I. Wisher, Developing a silica aerogel radiator for the HELIX ring-imaging Cherenkov system, Nucl. Instruments Methods Phys. Res. Sect. A Accel. Spectrometers, Detect. Assoc. Equip. 952 (2020), 161879, https://doi.org/10.1016/j.nima.2019.02.006.
[8] J.P. Vareda, L. Durães, Efficient adsorption of multiple heavy metals with tailored silica aerogel-like materials, Environ. Technol. 40 (2019) 529–541, https://doi.org/10.1080/09593330.2017.1397766.
[9] M.H. Sorour, H.A. Hani, G.A. Al-Bazedi, A.M. EL-Rafei, Hydrophobic silica aerogels for oil spills clean-up, synthesis, characterization and preliminary performance evaluation, J. Porous Mater. 23 (2016) 1401–1409, https://doi.org/10.1007/s10934-016-0200-5.
[10] N. Bheekhun, A. Rahim, A. Talib, M.R. Hassan, Aerogels in aerospace: a review, Adv. Mater. Sci. Eng. 2013 (2013).
[11] S.M. Jones, Aerogel: space exploration applications, J. Sol. Gel Sci. Technol. 40 (2006) 351–357, https://doi.org/10.1007/s10971-006-7762-7.
[12] K.E. Parmenter, F. Milstein, Mechanical properties of silica aerogels, J. Non-Cryst. Solids 223 (1998) 179–189, https://doi.org/10.1016/S0022-3093(97)00430-4.
[13] H. Maleki, L. Durães, A. Portugal, An overview on silica aerogels synthesis and different mechanical reinforcing strategies, J. Non-Cryst. Solids 385 (2014) 55–74, https://doi.org/10.1016/j.jnoncrysol.2013.10.017.
[14] S. Iswar, G.M.B.F. Snellings, S. Zhao, R. Erni, Y.K. Bahk, J. Wang, M. Lattuada, M.M. Koebel, W.J. Malfait, Reinforced and superinsulating silica aerogel through in situ cross-linking with silane terminated prepolymers, Acta Mater. 147 (2018) 322–328, https://doi.org/10.1016/j.actamat.2018.01.031.
[15] G. Zu, K. Kanamori, T. Shimizu, Y. Zhu, A. Maeno, H. Kaji, K. Nakanishi, J. Shen, Versatile double-cross-linking approach to transparent, machinable, supercompressible, highly bendable aerogel thermal superinsulators, Chem. Mater. 30 (2018) 2759–2770, https://doi.org/10.1021/acs.chemmater.8b00563.
[16] Z. Li, X. Cheng, S. He, X. Shi, L. Gong, H. Zhang, Aramid fibers reinforced silica aerogel composites with low thermal conductivity and improved mechanical performance, Compos. Part A Appl. Sci. Manuf. 84 (2016) 316–325, https://doi.org/10.1016/j.compositesa.2016.02.014.
[17] X. Tan, M. Yang, H.Y. Gao, Y. Luan, Z.K. Jin, N. A, Y.H. Feng, D.L. Feng, Preparation of fiber reinforced silica composite aerogel, Gongneng Cailiao/Journal Funct. Mater. 45 (2014) 16139–16142, https://doi.org/10.3969/j.issn.1001-9731.2014.16.030.
[18] R.B. Torres, J.P. Vareda, A. Lamy-Mendes, L. Durães, Effect of different silylation agents on the properties of ambient pressure dried and supercritically dried vinyl-modified silica aerogels, J. Supercrit. Fluids 147 (2019) 81–89, https://doi.org/10.1016/j.supflu.2019.02.010.
[19] T. Linhares, M.T. Pessoa De Amorim, L. Durães, Silica aerogel composites with embedded fibres: a review on their preparation, properties and applications, J. Mater. Chem. A. 7 (2019) 22768–22802, https://doi.org/10.1039/c9ta04811a.
[20] A. Lamy-Mendes, W.J. Malfait, A. Sadeghpour, A.V. Girão, R.F. Silva, L. Durães, Influence of 1D and 2D carbon nanostructures in silica-based aerogels, Carbon N. Y. 180 (2021) 146–162, https://doi.org/10.1016/j.carbon.2021.05.004.
[21] M. Piñero, M.M. Mesa-Díaz, D. de los Santos, M.V. Reyes-Peces, J.A. Díaz-Fraile, N. de la Rosa-Fox, L. Esquivias, V. Morales-Florez, Reinforced silica-carbon nanotube monolithic aerogels synthesised by rapid controlled gelation, J. Sol. Gel Sci. Technol. 86 (2018) 391–399, https://doi.org/10.1007/s10971-018-4645-7.
[22] S.K. Adhikary, Ž. Rudžionis, S. Tučkutė, D.K. Ashish, Effects of carbon nanotubes on expanded glass and silica aerogel based lightweight concrete, Sci. Rep. 11 (2021) 1–11, https://doi.org/10.1038/s41598-021-81665-y.
[23] M. Schwan, M. Rößler, B. Milow, L. Ratke, From Fragile to Resilient Insulation : Synthesis and Characterization of Aramid-Honeycomb Reinforced Silica Aerogel Composite Materials, 2016, https://doi.org/10.3390/gels2010001.
[24] Y. Liu, Z. Chen, J. Zhang, S. Ai, H. Tang, Ultralight and thermal insulation carbon foam/SiO2 aerogel composites, J. Porous Mater. 26 (2019) 1305–1312, https://doi.org/10.1007/s10934-019-00732-y.
[25] X. Ye, Z. Chen, S. Ai, B. Hou, J. Zhang, Q. Zhou, F. Wang, H. Liu, S. Cui, Microstructure characterization and thermal performance of reticulated SiC skeleton reinforced silica aerogel composites, Compos. Part B. 177 (2019), 107409, https://doi.org/10.1016/j.compositesb.2019.107409.

[26] O. Doutres, N. Atalla, K. Dong, Effect of the microstructure closed pore content on the acoustic behavior of polyurethane foams, J. Appl. Phys. 110 (2011), https://doi.org/10.1063/1.3631021.
[27] ASTM D1622-08: Standard Test Method for Apparent Density of Rigid Cellular Plastics, ASTM International, West Conshohocken, PA, USA, 2008, https://doi.org/10.1520/D1622-20.
[28] A. Ayral, J. Phalippou, T. Woignier, Skeletal density of silica aerogels determined by helium pycnometry, J. Mater. Sci. 27 (1992) 1166–1170, https://doi.org/10.1007/BF01142014.
[29] E.P. Barrett, L.G. Joyner, P.P. Halenda, The determination of pore volume and area distributions in porous substances. I. Computations from nitrogen isotherms, J. Am. Chem. Soc. 73 (1951) 373–380, https://doi.org/10.1021/ja01145a126.
[30] L. Juhász, K. Moldován, P. Gurikov, F. Liebner, I. Fábián, J. Kalmár, C. Cserháti, False morphology of aerogels caused by gold coating for sem imaging, Polymers 13 (2021) 1–12, https://doi.org/10.3390/polym13040588.
[31] J. Pinto, E. Solórzano, M.A. Rodriguez-Perez, J.A. De Saja, Characterization of the cellular structure based on user-interactive image analysis procedures, J. Cell. Plast. 49 (2013) 555–575, https://doi.org/10.1177/0021955X13503847.
[32] J. Bhinder, P.K. Agnihotri, Effect of carbon nanotube doping on the energy dissipation and rate dependent deformation behavior of polyurethane foams, J. Cell. Plast. (2020), https://doi.org/10.1177/0021955X20917280.
[33] ASTM C518- Standard Test Method for Steady-State Thermal Transmission Properties by Means of the Heat Flow Meter Apparatus, 2017. West Conshohocken, PA, USA.
[34] ISO 8301:1991- Thermal Insulation — Determination of Steady-State Thermal Resistance and Related Properties — Heat Flow Meter Apparatus, 1991. Geneva, Switzerland.
[35] I. Sánchez-Calderón, B. Merillas, V. Bernardo, M.Á. Rodríguez-Pérez, Methodology for measuring the thermal conductivity of insulating samples with small dimensions by heat flow meter technique, J. Therm. Anal. Calorim. (2022), https://doi.org/10.1007/s10973-022-11457-7.
[36] B. Merillas, J.P. Vareda, J. Martín-de León, M.Á. Rodríguez-Pérez, L. Durães, Thermal conductivity of nanoporous materials : where is the limit ? Polymers (Basel) 14 (2022).
[37] B. Notario, J. Pinto, E. Solorzano, J.A. De Saja, M. Dumon, M.A. Rodríguez-Pérez, Experimental validation of the Knudsen effect in nanocellular polymeric foams, Polymer (Guildf) 56 (2015) 57–67, https://doi.org/10.1016/j.polymer.2014.10.006.